Thermodynamic Re-assessment of the Nb-Zr System Using the CE–CVM Model for Solid Solution Phases

Shanker Kumar[1] · Vikas Jindal[1]

Abstract The Nb-Zr system was reassessed based on calculated theoretical data and available thermodynamic and phase equilibria data. The Gibbs energies of the bcc and hcp solid phases were described using cluster expansion and cluster variation methods (CE–CVM) to model short-range ordering (SRO) in the solid solution phases. Enthalpy of mixing data was calculated using density functional theory with special quasirandom structures and cluster expansion (CE) method. A sub-regular solution model was used for describing the Gibbs energy of the liquid phase. An optimal set of parameters has been obtained for describing the Gibbs energies of the liquid and solid phases in the Nb-Zr binary system. The modeled phase diagram and thermodynamic properties agree with the experimental data. The relevance of CE–CVM has been demonstrated in the present case by calculating the solid phase's short-range order (SRO) parameters as a function of composition and temperature.

Keywords CALPHAD method · computational thermodynamics · cluster variation method · Nb-Zr system · phase diagram · thermodynamic assessment

1 Introduction

Niobium and zirconium are important alloying elements for superalloys and refractory alloys. Nb-Zr alloys exhibit excellent mechanical properties, superior corrosion resistance, low magnetic susceptibility, superconducting nature, and superior irradiation resistance. They can also be used in biomedical applications such as knee and hip replacement for orthopedic surgeries due to their biocompatibility.[1] The Nb-Zr phase diagram is vital to understanding these alloys' structure and properties at various temperatures and compositions. Many efforts have been made to determine the phase diagram of this system, which were reviewed by Abriata and Bolcich[2](1982) and Guillermet.[3] In this system, there is complete miscibility in the liquid state, and the liquidus and solidus show a minimum point where the bcc_A2 (β) phase melts congruently. At high temperatures, the bcc_A2 phase covers the whole compositional range. In contrast, it exhibits a critical solution point at lower temperatures and a corresponding (βZr) + (βNb) miscibility gap. There is a monotectoid reaction (βZr) ↔ (αZr) + (βNb), which results in the coexistence of hcp_A3 (αZr) with (βNb). The solidus and the liquidus were measured by Rogers and Atkins[4] and Lundin and Cox.[5] Flewitt[6] and Van Effenterre[7] data are preferred for the miscibility gap. The solubility limits in the temperature range of interest are mainly based on the x-ray analysis of Flewitt[6] for the Nb-rich part and the experimental data (x-ray, resistivity, microscopical examination, and dilatometry) of Van Effenterre for the Zr-rich part.[7] No reliable experimental thermodynamic data is available for this system.[2] Thermodynamic assessments of the Nb-Zr system have been done by Abriata and Bolcich,[2] Guillermet,[3] Lafaye et al.[8] In these assessments, the Gibbs energy of phases is described using the sublattice

✉ Vikas Jindal
vijindal@gmail.com

1 Department of Metallurgical Engineering, Indian Institute of Technology (Banaras Hindu University), Varanasi 221005, India

model within the Compound Energy Formalism framework (CEF).

The reliability of thermodynamic modeling depends on the quantity and quality of data used to evaluate thermodynamic model parameters.[9,10] Two sets of input data are used in the CALPHAD modeling: thermochemical data and phase equilibrium data. Measuring reliable thermochemical data such as enthalpy of mixing is very challenging compared to phase equilibrium data. Limited solubility range and sluggish kinetics at low temperatures limit the reliability of these measurements. Hence, the first-principles calculations can be used instead of experiments for determining thermochemical data. Density functional theory (DFT), along with techniques such as cluster expansion[11] and Special Quasirandom Structures (SQS),[12–15] can be used to calculate thermochemical data. Cottura and Clouet[16] studied the solubility of the Zr-Nb system temperatures below 890 K using DFT. Barannikova et al.[17] computed mixing enthalpies for hcp_A3, bcc_A2, and hypothetical fcc Zr-Nb alloys using ab initio methods. An interatomic potential for simulation of Zr-Nb system was reported by Smirnova and Starikov.[18] Zhao et al.[19] studied bcc_A2 ordered and disordered Nb-Zr systems using the first-principles method and reported positive formation energy in bcc_A2 Zr-Nb alloy. For lower Nb concentration (≤ 12.5 at.%), the bcc_A2 Zr-Nb solid solution structure was unstable. Natarajan et al.[20] have reported a cluster expansion (CE) study of this system. However, available thermodynamic descriptions of the Nb-Zr system have not used calculated thermochemical data so far in the assessments.

It is well known that the constituent atoms of an alloy are not distributed randomly over the crystal lattice sites. Instead, depending on the atomic interaction energies, the different kinds of atoms tend to distribute in a non-random way as the temperature is lowered. This deviation from the random distribution is known as SRO, and it influences several physical parameters, including mechanical, electrical, and magnetic properties.[21] The presence of SRO also decreases the configurational entropy from ideal estimates. This is important for the thermal stability of high entropy alloys (HEA) which are based on the concept that their high configurational entropy of mixing should stabilize simple solid-solution phases (such as fcc or bcc) relative to other competing phases. Hence thermodynamic descriptions and databases which take SRO into account are highly desirable. Several models have been developed to describe the effect of SRO, e.g., the cluster variation method (CVM)[11] and Monte Carlo (MC) techniques.[20] One of the significant advantages of these techniques is that Gibbs energy is expressed directly in terms of SRO parameters.

Re-assessment of the Nb-Zr system is desirable for two reasons: (1) to incorporate newly available thermochemical data based on first-principle calculations and (2) to model SRO present in the solid solution phases. Enthalpy of mixing data of the solid solution phases will be calculated using DFT calculations with SQS and cluster expansion methods. All the available experimental and calculated data will be optimized to get a thermodynamic description of the system.

2 Methodology

2.1 DFT Calculations

Electronic structure total energy calculations[22] of ordered configurations, required for the construction of the cluster expansion Hamiltonian, were performed using Quantum-Espresso[23–25] (with the generalized gradient approximation (GGA).[26,27] Ultra-soft pseudopotentials[28,29] with an energy cutoff of 400 eV were used. The first-order Methfessel-Paxton[30] method of electronic occupancy was used with a smearing width of 0.2 eV. Brillouin zone integration was carried out using a Monkhorst- Pack k-point mesh. In this work, the k-point density per reciprocal atom (KPPRA) was set to 46656, which, for the bcc_A2 structure, translates to a $36 \times 36 \times 36$ grid. These choices of basis cutoff and k-point grid ensure convergence of the total energy within a few meV/atom.

2.2 SQS Calculations

The SQS method was used to determine the mixing enthalpies of the bcc_A2 solid solution. As mentioned earlier, this method generates a series of "special" configurations that reproduce the random disorder of a solid solution at a given composition with a limited number of atoms per unit cell. The present work generated the bcc_A2 structures for 0.25, 0.50, and 0.75 binary compositions using 16-atom supercells.[14] The mixing enthalpy was calculated by subtracting the total energy of the SQS structure calculated by DFT to the molar fraction weighted sum of the energies of the pure elements in a structure similar to the solid solution structure. SQS supercells were relaxed in two ways: (1) relaxed with respect to cell volume only and (2) fully relaxed. Relaxed SQS structures were checked for symmetry.

2.3 Cluster Expansion

In the cluster expansion method, any function of configuration for a phase, such as the configurational enthalpy H_c, can be expressed as a bilinear sum of the products of the

correlation functions and their respective cluster expansion coefficients (CECs). This idea is very analogous to a Taylor or Fourier expansion.

The function H_c can be expressed as[11,31]

$$H_c = \sum_{j=1}^{r_N} C_j m_j u_j \qquad \text{(Eq 1)}$$

Here, the subscript j is an index that serves to identify each distinct cluster type r_N is the number of all distinct cluster types, C_j are the CECs and m_j, the multiplicities corresponding to the respective correlation functions u_j. The multiplicities m_j are defined as the number of symmetry−equivalent clusters of type j per site present in the structure.

The Alloy Theory Automated Toolkit (ATAT)[37] was used to construct the cluster expansion Hamiltonian for the bcc_A2 structure. Energies of the structures generated by ATAT were calculated using Quantum-Espresso. To find the optimum set of ECIs, we use a database of DFT energies computed for 110 bcc_A2-like structures. DFT calculations involve full atomic relaxations.

2.4 Thermodynamic Models

2.4.1 Pure Elements

The enthalpy of a pure component i at 298.15 K, 1 bar pressure, and at its the stable state (say $\emptyset$) is denoted as Stable Element Reference, H_i^{SER}. And with reference to this H_i^{SER}, the Gibbs energy of component i in the phase $\emptyset$ is described as a function of temperature by the following expression[32]:

$$G_i^{\emptyset,0}(T) - H_i^{SER} = a + bT + cT \ln T + \sum dT^n \qquad \text{(Eq 2)}$$

where a, b, c, and d are coefficients and n represents a set of integers, typically taking the values of 2, 3, and -1. The Gibbs energy functions for the unary phases of pure elements Nb and Zr are selected from the Scientific Group Thermodata Europe (SGTE) database.[32]

2.4.2 Solution Phases

Gibbs energy of a given phase $\emptyset$ can be written as the sum of the reference energy term $G^{\emptyset,ref}$ and mixing energy term $G^{\emptyset,mix}$ in a given solution.

$$G^{\emptyset} = G^{\emptyset,ref} + G^{\emptyset,mix} \qquad \text{(Eq 3)}$$

The reference energy term can be expressed as Gibbs energy of pure elements

$$G^{\emptyset,ref} = x_{Nb} G_{Nb}^{\emptyset,0} + x_V G_{Zr}^{\emptyset,0} \qquad \text{(Eq 4)}$$

The mixing energy term can be further split into terms

$$G^{\emptyset,mix} = G^{\emptyset,id} + G^{\emptyset,xs} \qquad \text{(Eq 5)}$$

The ideal part of the equation can be expressed as

$$G^{\emptyset,id} = RT(x_{Nb} \ln x_{Nb} + x_{Zr} \ln x_{Zr}) \qquad \text{(Eq 6)}$$

where x_{Nb} and x_{Zr} are mole fractions of Nb and Zr in the solution phase. There are two solution phases in the system: liquid and bcc_A2. The liquid phase of the given system has been modeled using Redlich-Kister polynomial expansion[33] using the following equation:

$$G^{l,xs} = x_{Nb} x_{Zr} \left(L_0^l(T) + L_1^l(T)(x_{Nb} - x_{Zr}) + L_2^l(T)(x_{Nb} - x_{Zr})^2 + \dots \right)$$

and

$$L_i^l = L_{i0}^l + L_{i1}^l T \qquad \text{(Eq 7)}$$

where L_i^l is the ith interaction parameter.

The bcc_A2 and hcp_A3 phases were treated using phenomenological cluster expansion (CE) for configurational enthalpy of mixing and CVM for configurational entropy of mixing.[34] The tetrahedron and tetrahedron-octahedron approximations of the CE-CVM were used for the bcc_A2 and hcp_A3 phases, respectively. Both these models take into account interactions up to second nearest-neighbor pairs. Further details are given in the supplementary data. The Gibbs energy of mixing for the bcc_A2 phase is expressed as

$$G^{\beta,mix} = H^{\beta,mix} - TS^{\beta,mix} \qquad \text{(Eq 8)}$$

where $H^{\beta,mix}$ and $S^{\beta,mix}$ respectively denote the enthalpy and entropy of mixing.

$$H^{\beta,mix} = \sum_i C_i^{\beta} m_i^{\beta} u_i^{\beta,mix} \qquad \text{(Eq 9)}$$

$$S^{\beta,mix} = -R \sum_i \gamma_i^{\beta} m_i^{\beta} \sum_j w_{i,j} \rho_{i,j} \ln \rho_{i,j} \qquad \text{(Eq 10)}$$

$$C_i^{\beta} = C_{i0}^{\beta} + C_{i1}^{\beta} T \qquad \text{(Eq 11)}$$

The C_i^{β} are phenomenological cluster expansion coefficients (CECs) or effective cluster interactions (ECIs), which may be temperature-dependent. The subscript i refers to one of the five crystallographically distinct clusters for the tetrahedron approximation. The multiplicity m_i^{β} is equal to the number of clusters of type i per atomic site in the structure and $u_i^{\beta,mix} = u_i^{\beta} - x_{Nb} u_{i,Nb}^{\beta} - x_V u_{i,Zr}^{\beta}$. Here u_i^{β}, $u_{i,Nb}^{\beta}$ and $u_{i,Zr}^{\beta}$ represent the correlation functions corresponding to cluster type i for the alloy, pure Nb and pure Zr, respectively. These correlation functions are the average values of site operators or their products. In the orthogonal basis we use, the site operator takes the value

280

J. Phase Equilib. Diffus. (2022) 43:277–286

−1 or +1, respectively, when component Nb or Zr atom occupies the site.[35] Further, γ_i^β is the Kikuchi–Barker overlap correction coefficient for cluster type i. The cluster variable $\rho_{i,j}$ represents the probability of occurrence of cluster configuration j on cluster type i and $w_{i,j}$ represents the weight of cluster configuration j. These cluster variables are, in turn, functions of correlation functions $\rho_{i,j} = \rho_{i,j}\left(u_i^\beta\right)$. The Gibbs energy of the phase, parameterized by C_i^β, can be obtained by minimizing it with respect to the correlation functions[35] using the Newton–Raphson (NR) method. The model parameters L_i^l and C_i^β can be obtained by simultaneous optimization of all available experimental data for the system.

2.5 Simultaneous Optimization

In the present work, all available phase diagrams and thermodynamic data have been simultaneously optimized with equal weights using the procedure given by Lele and Sarma.[35] The simultaneous optimization procedure begins by defining a figure-of-merit function (χ^2) as the sum (over all N data points) of squares of the ratios of the errors ε_i and the respective standard deviations σ_i. Thus,

$$\chi^2 = \sum_{i=1}^{N}\left(\frac{\varepsilon_i}{\sigma_i}\right)^2 \tag{Eq 12}$$

In general, ε_i corresponds to the difference between the observed quantity and that calculated using the model under the conditions of experimentation. The χ^2-merit function is minimized with respect to a chosen set of model parameters to determine their values using the Levenberg–Marquardt (LM) algorithm.[36] We developed necessary computer codes for optimization following the algorithmic considerations discussed by Press et al.[36] Details of the procedure are given in Ref. 37

3 Results and Discussion

3.1 DFT Calculations

The lattice parameters are compared with experimental values to benchmark our first-principles calculations. Table 1 shows the lattice parameter, equilibrium volume, and bulk modulus comparisons for the pure elements. For the pure elements, comparisons are also made to DFT results calculated by Lejaeghere et al.[38] Good agreement between the experiment and DFT calculation was observed.

3.2 SQS Calculations

Nb and Zr form a continuous bcc_A2 solid solution with a miscibility gap appearing at low temperatures. In Fig. 1, the calculated enthalpies of mixing for random Nb-Zr bcc_A2 alloys using volume relaxed and fully relaxed SQS structures are shown. As expected, energies for the fully relaxed are found to be lower than volume relaxed structures. Values of relaxed SQS structures compare well with the work of Colinet et al.,[42] Lafaye et al.,[8] and Zhao et al.,[19] except near the Zr end. Overall, the enthalpy of mixing is positive and indicates that Nb-Zr is a phase separating-type system. This is consistent with experimental findings where bcc_A2 shows a miscibility gap at lower temperatures. However, enthalpy of mixing for x_{Zr} = 0.75 is found to be negative. Zhao et al.[19] have also reported similar results near the Zr end. Negative values near the Zr end may be attributed to the bcc Zr-Nb alloy being a dynamically unstable system.

3.3 Cluster Expansion

The bcc_A2 structure is chosen for the Nb-Zr system to perform CE calculations as parent lattices. The comparison of the enthalpy of formation obtained from the DFT calculations and the CE method is shown in Fig. 2. there is a good agreement between these two methods, as shown in the figure. The CV score of the present calculation is 0.00806828 and sufficiently small for the CE method.[43] Figure 3(a) shows the calculated and fitted energy of the structures used in cluster expansion. The cluster expansion has predicted one ground state belonging to space group C2/m (12). The formation enthalpy of this ground-state is small, less than − 16 meV/atom. Calculated effective cluster interaction (ECI) versus cluster diameter plots are given in Fig. 3(b). Values are three-point, and four-point ECIs are smaller than pair ECIs, and convergence of ECIs can be readily observed. To analyze ECIs, the ECIs of the empty, the point, the first two nearest pairs, and the first triplet, which includes the nearest pair, are listed in Table 2. The ECI value of the empty cluster corresponds to the energy of the fully-disordered alloy. A large positive value of the fully-disordered alloy indicates its instability, which is consistent with positive values of mixing obtained from SQS calculation and the observed miscibility gap in the bcc phase.[44] It may be noted from Table 2 that the ECIs of the nearest and second nearest pair cluster for bcc are negative. This further indicated tendency for the phase separation in the bcc phase. The energy of the disordered bcc phase at various compositions has been calculated using fitted ECIs, and these results are shown in Fig. 3(a). Predicted enthalpy of mixing from CE match well with the SQS method (Fig. 2).

Table 1 Comparison of equilibrium bulk properties of Nb (in bcc_A2) and Zr (in bcc_A2 and hcp_A3) as calculated with DFT calculations and their respective experimental values.

Element	Bulk property	This Work	Experimental	DFT
β-Nb	Lattice parameter, Å	3.3088	3.299[39]	3.3084[38]
	Equilibrium volume, Å³/atom	18.11	17.952[39]	18.106[38]
	Bulk modulus, GPa	170	170.2[39]	170.28[38]
α-Zr	Lattice parameter, Å	…	a = 3.233, c = 5.146[40]	…
	Equilibrium volume, Å³/atom	23.385	23.285[40]	23.383[38]
	Bulk modulus, GPa	93.7	94[40]	93.885[38]
β-Zr	Lattice parameter, Å	3.6665	3.627*[40]	3.574[41]
	Equilibrium volume, Å³/atom	24.64	23.857*[40]	22.826[41]
	Bulk modulus, GPa	87.9	66*[40]	90.2[41]
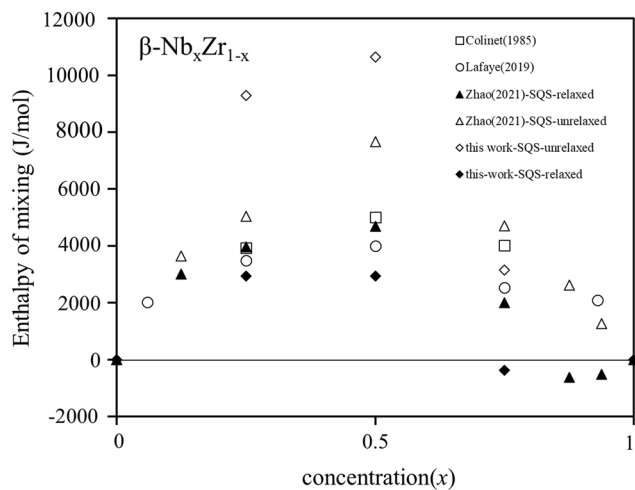
Fig. 1 Calculated mixing enthalpies of the bcc_A2 solid solutions in the Nb-Zr system compared to data from the literature

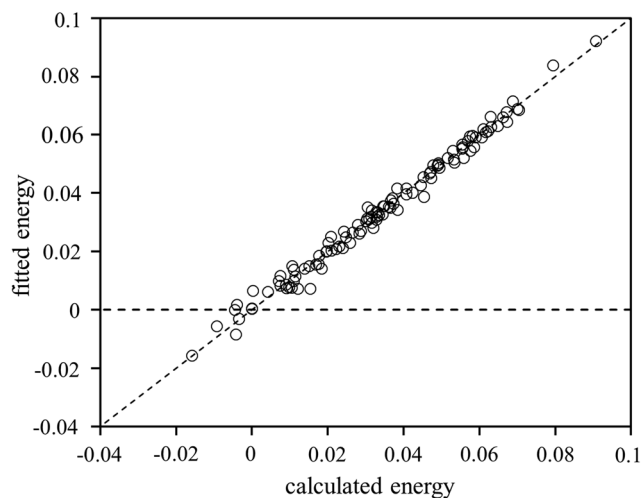**Fig. 2** Comparison of enthalpies of formation (eV/atom) obtained from first principle calculations and predicted with the CE method
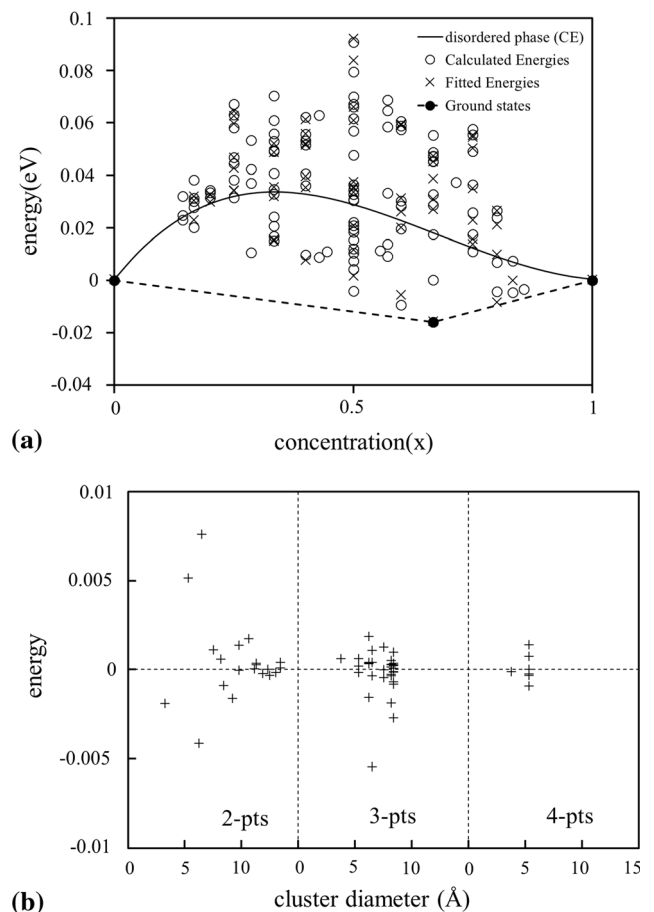

Fig. 3 (a) Ground-state search for the cluster expansion of Nb-Zr bcc_A2 phases in (a) and (b) ECI vs. cluster diameter for a cluster expansion fit to the as calculated first principles energies

3.4 Simultaneous Optimization

As mentioned earlier, the phase diagram Nb-Zr system is characterized by three invariant reactions: congruent melting, critical point of miscibility gap, and monotectoid. For congruent melting, temperature and composition values observed by Ref. 4 and [5] are in good agreement, and the same values have been used in this work. A dataset

282

J. Phase Equilib. Diffus. (2022) 43:277–286

similar to Guillermet[3] was used for liquidus and solidus boundaries. The consolute point and monotectoid temperature values of Flewitt[6] have been accepted for this work. These three invariant reaction data points have been given more weightage during the optimization. First, parameters for the bcc phase have been optimized using the miscibility gap and enthalpy of mixing data. With optimized bcc phase parameters, hcp phase parameters have been optimized using bcc-hcp phase equilibria data. Next, liquid phase parameters have been optimized using liquid and solidus data with optimized bcc phase parameters. Lastly, the entire parameter set is further refined with the complete dataset. The number of optimization parameters in the procedure described in the previous section was gradually increased till all systematic deviations of the calculated values from the observed ones were eliminated. Efforts were made to keep the number of parameters minimum. The optimized parameters, along with those from previous assessments, are given in Table 3. It is found that a reasonably good description of the Gibbs energy for the bcc phase may be obtained by using parameters related to the first, second neighbor pair, and triangle only. The second neighbor pair cluster expansion coefficient (CEC) is fixed as 2/3rd of the first neighbor CEC since independent optimization of these parameters often leads to non-

Table 2 Selected ECIs for Nb-Zr bcc system

Num of sites	Multiplicity	ECI, eV	ECI, J/mol
0	1	0.028932	2791.694
1	1	− 0.026241	− 2532.0352
2	4	− 0.001906	− 183.9129
2	3	− 0.010107	− 975.2403
3	12	0.00061	58.8599
4	6	− 0.000116	− 11.193

Table 3 Optimized set of ECI's used in assessing the Nb-Zr phase diagram

Phase	Parameters, J/mol
bcc_A2 phase	$C_2^\beta = -462.6 - 0.4152 * T$ (I-neighbor pair)
	$C_3^\beta = -308.4 - 0.2768 * T$ (II-neighbor pair)
	$C_4^\beta = 88.0$ (Triangle)
hcp_A3	$C_2^\alpha = -841.4$ (I-neighbor pair)
	$C_3^\alpha = -841.4$ (II-neighbor pair)
Liquid	$L_0^l = -28060.0 + 21.72*T$
	$L_1^l = -24650 + 10*T$

physical values. Temperature dependence of some parameters was needed to fit experimental data. For the hcp phase, the minimal set consists of the first neighbor pair interactions (with the CECs corresponding to the in-plane and out-of-plane first neighbors being equal, $C_2^\alpha = C_3^\alpha$, that is, the interactions were assumed to be isotropic). Due to the different modeling approaches, the model parameters cannot be compared with earlier assessments.

The calculated phase diagram is shown in Fig. 4. A comparison with the numerous experimental data on the solidus and liquidus is given in Fig. 5, and a reasonably good agreement with the experimental data may be seen. At lower temperatures, phase decomposition has been observed. Figure 6 shows the calculated miscibility gap boundary and monotectoid reaction with experimental information. Reasonable compliance between them may be observed. The invariant points in the phase diagram are presented in Table 4, along with earlier results. There is good agreement among all the results.

Enthalpies of mixing have been calculated at two temperatures, as shown in Fig. 7. Calculated enthalpies of mixing are compared with those obtained from cluster expansion and SQS. Overall good agreement is found with cluster expansion results. However, SQS values show deviations from the calculated values near the Zr end.

As mentioned earlier, SRO can be determined using CVM. A quantitative measure of SRO is provided by the Cowley-Warren SRO parameters α_i,[45] which can be calculated from

$$\alpha_i = \frac{u_i - u_0^2}{1 - u_0^2} \quad \text{(Eq 13)}$$

Here u_i and u_0 are the equilibrium values of the ith pair and point correlation functions, respectively. The variation of the first neighbor SRO as a function of composition for
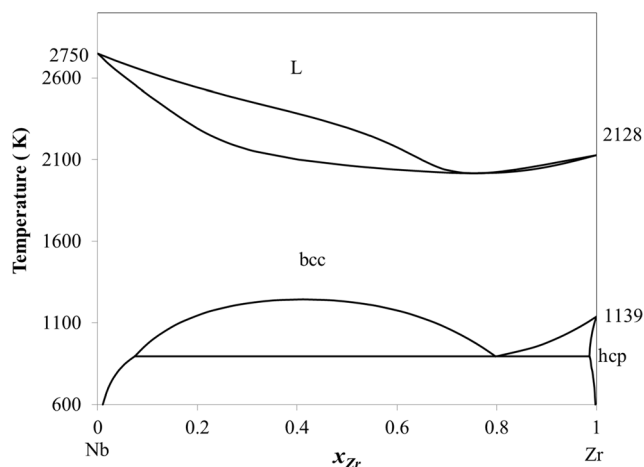

Fig. 4 Calculated phase diagram and invariant points of Nb-Zr system
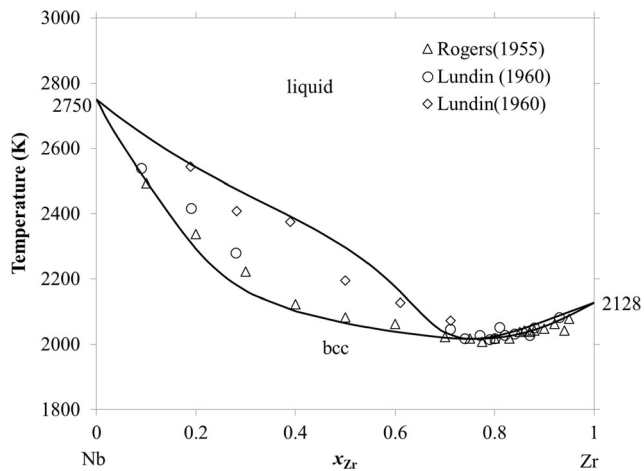
Fig. 5 Calculated liquidus and solidus boundaries in the Nb-Zr system along with experimental data
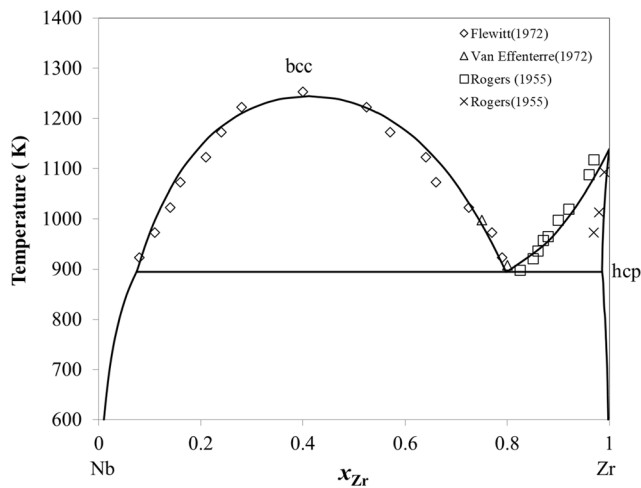

Fig. 6 Calculated miscibility gap and monotectiod reaction in the solid phase (solid line) and experimental data

Fig. 7 Calculated enthalpy of mixing of the solid phase at 1900 K along with calculated data in this work

various temperatures is shown in Fig. 8. A considerable degree of SRO may be seen particularly near the miscibility gap boundary and at lower temperatures. Similarly, the variations of the SRO parameter with temperature for the first nearest neighbor pair for the 25, 50, and 75 at.% alloys are shown in Fig. 9. As expected, the maximum degree of SRO is observed at lower temperatures and decreases with temperature. The persistence of SRO even at high temperatures justifies using thermodynamic models which account for SRO. Another useful application of CVM can be seen in analyzing the effect of SRO on configurational entropy of mixing. Variation of configurational entropy with composition at various temperatures is shown in Fig. 10. Configurational entropy, as expected, shows higher values near equiatomic alloys. However, these values are considerably smaller than those calculated from the ideal entropy of mixing due to the presence of SRO.
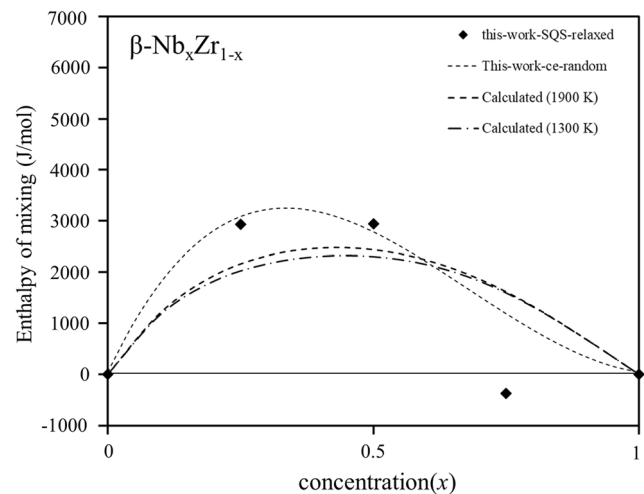
Secondly, compositions corresponding to maximum configurational entropy are not equiatomic compositions. These are important observations from the point of view of designing stable HEA compositions. Contrary to the simplistic ideal entropy of the mixing model, the CE-CVM model better estimates the entropy of mixing and locating compositions that maximize them. This information is crucial in the determination of the stability of the HEAs.
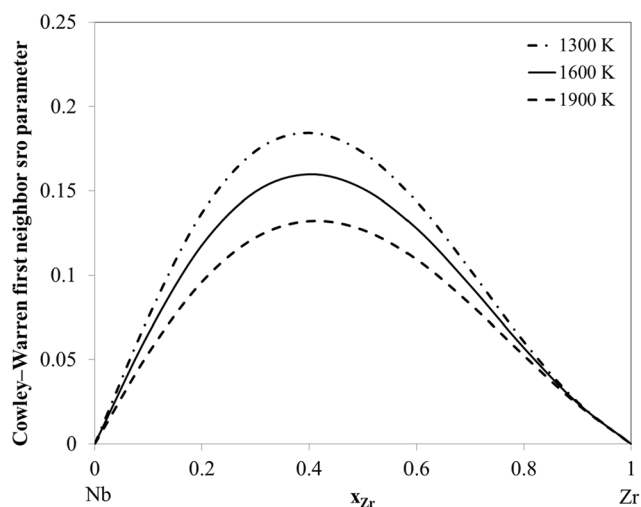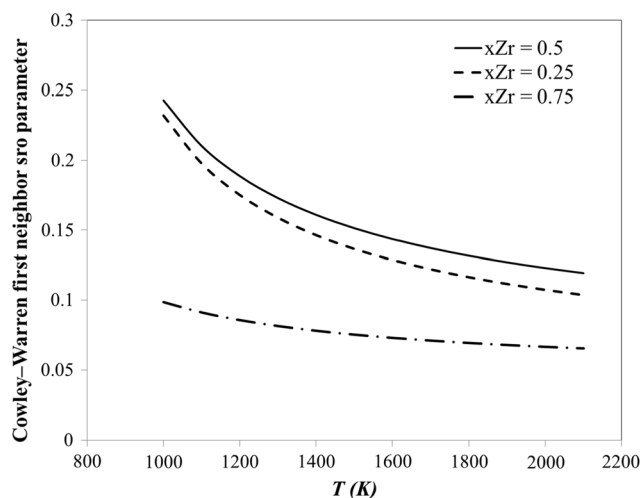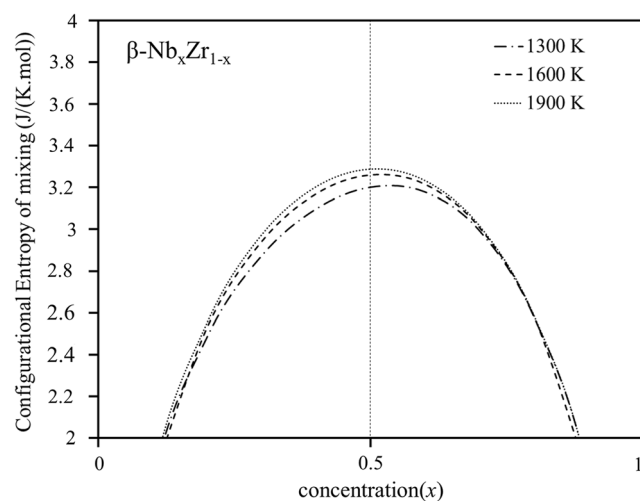
Comparing CEC parameters of the bcc phase obtained after optimization with those obtained from cluster expansion will be interesting. CE and optimized CECs of both first and second neighbor pairs are negative. A direct comparison is not possible due to the temperature dependence of optimized CECs parameters. It may be noticed that the value of the first neighbor CEC is lower than that of the second neighbor in the case of CE. This is slightly unphysical and difficult to avoid in CE fitting. However, during simultaneous data optimization in this work, the second neighbor pair CEC is fixed as 2/3rd of the first neighbor CEC to avoid this kind of anomaly. CEC values of the triangle cluster obtained from both approaches are positive and compare well. Cluster expansion CEC corresponding to the four-point cluster is negligible compared to pair CECs and not used in optimization. Overall a qualitative agreement may be observed in both the parameters set.

4 Conclusions

This study aimed to reassess the Nb-Zr system using newly available calculated thermochemical data and employing the CE-CVM model for the solid solution phases for modeling SRO. Enthalpy of mixing for the Nb-Zr bcc

Table 4 Invariant points in the Nb-Zr system

Invariants	Ref. [6]		Ref. [2]		Ref. [3]		Present work	
	T, K	x_{Zr}	T, K	x_{Zr}	T, K	x_{Zr}	T, K	x_{Zr}
Congruent minimum	…	…	2013	0.783	2016	0.782	2017	0.755
Consolute point	1253	0.40	1261	0.394	1250	0.413	1245	0.412
Three-phase equilibrium	893	0.10 (βNb)	893	0.09 (βNb)	893	0.079 (βNb)	895	0.074 (βNb)
		0.85 (βZr)		0.815 (βZr)		0.813 (βZr)		0.797 (βZr)
		- (αZr)		0.994 (αZr)		0.993 (αZr)		0.986 (αZr)

Fig. 8 Calculated Cowley–Warren first neighbor SRO parameter for the bcc_A2 phase as a function of composition at different temperatures

Fig. 10 Variation of configurational entropy of mixing with composition for the bcc solid phase at various temperatures

solutions calculated using DFT calculation with (1) SQS and (2) cluster expansion methods. Both methods have given similar results. A consistent set of thermodynamic parameters has been arrived at for describing the Gibbs energies of the solid and liquid solution phases, leading to good agreement between the calculated results and most of the experimental data found in the literature. Cowley–Warren's first neighbor SRO parameters were calculated for the bcc phase. A considerable amount of sro was found at low temperatures and equiatomic compositions. Present work is a step towards modeling SRO in the multi-principal HEA alloys.

Fig. 9 Calculated Cowley–Warren first neighbor SRO parameters for the bcc_A2 phase as a function of temperature for various compositions

Conflict of interest The authors declare that they have no known competing financial interests or personal relationships that could have appeared to influence the work reported in this paper.

References

1. F.Y. Zhou, B.L. Wang, K.J. Qiu, W.J. Lin, L. Li, Y.B. Wang, F.L. Nie, and Y.F. Zheng, Microstructure, Corrosion Behavior and Cytotoxicity of Zr-Nb Alloys for Biomedical Application, *Mater. Sci. Eng. C*, 2012, **32**(4), p 851-857. https://doi.org/10.1016/j.msec.2012.02.002

2. J.P. Abriata, and J.C. Bolcich, The Nb-Zr (Niobium-Zirconium) System, *Bull. Alloy Phase Diagrams*, 1982, **3**(1), p 34-44.

3. A. Fernandez Guillermet, Thermodynamic Analysis of the Stable Phases in the Zr-Nb System and Calculation of the Phase Diagram, *Zeitschrift fuer Met. Res. Adv. Tech.*, 1991, **82**(6), p 478-487.

4. B.A. Rogers, and D.F. Atkins, Zirconium-Columbium Diagram, *JOM*, 1955, **7**(9), p 1034-1041. https://doi.org/10.1007/BF03377608

5. C.E. Lundin and R.H. Cox, The Determination of the Equilibrium Phase Diagram Zirconium-Niobium, U. S. Atomic Energy Commission, TID-11919 (1960).

6. P.E.J. Flewitt, A Re-Assessment of the Monotectoid Loop (β-Nb+β-Zr) in the Niobium-Zirconium System, *J. Appl. Crystallogr.*, 1972, **5**(6), p 423-425. https://doi.org/10.1107/S0021889872010076

7. V. Effenterre, Etude Du Diagramme d'équilibre et Des Transformations Structurales Obtenues Par Trempe à Vitesse Variable Ou Par Revenu Dans Les Alliages de Zirconium-Niobium (0-55% Nb), Univ. Paris Sud Orsay, CEA Saclay, France, 1972.

8. P. Lafaye, C. Toffolon-Masclet, J.-C. Crivello, and J.-M. Joubert, Experimental Investigations and Thermodynamic Modelling of the Cr-Nb-Sn-Zr System, *Calphad*, 2019, **64**, p 43-54. https://doi.org/10.1016/j.calphad.2018.11.002

9. L. Kaufman and H. Bernstein, *Computer Calculation of Phase Diagrams*. Academic Press, New York, 1970.

10. N. Saunders and A.P. Miodownik, CALPHAD (Calculation of Phase Diagrams): A Comprehensive Guide, in *Pergamon Materials Series* (Elsevier Science Ltd, 1998).

11. J.M.M. Sanchez, F. Ducastelle, and D. Gratias, Generalized Cluster Description of Multicomponent Systems, *Phys. A Stat. Mech. its Appl.*, 1984, **128**(1-2), p 334-350. https://doi.org/10.1016/0378-4371(84)90096-7

12. A. Zunger, S.H. Wei, L.G. Ferreira, and J.E. Bernard, Special Quasirandom Structures, *Phys. Rev. Lett.*, 1990, **65**(3), p 353-356.

13. S.H. Wei, L.G. Ferreira, J.E. Bernard, and A. Zunger, Electronic Properties of Random Alloys: Special Quasirandom Structures, *Phys. Rev. B*, 1990, **42**(15), p 9622-9649.

14. C. Jiang, C. Wolverton, J. Sofo, L. Chen, and Z. Liu, First-Principles Study of Binary Bcc Alloys Using Special Quasirandom Structures, *Phys. Rev. B*, 2004, **69**(21), p 214202. https://doi.org/10.1103/PhysRevB.69.214202

15. D. Shin, R. Arróyave, Z.K. Liu, and A. Van De Walle, Thermodynamic Properties of Binary Hcp Solution Phases from Special Quasirandom Structures, *Phys. Rev. B Condens. Matter Mater. Phys.*, 2006, **74**(2), p 1-13.

16. M. Cottura, and E. Clouet, Solubility in Zr-Nb Alloys from First-Principles, *Acta Mater.*, 2018, **144**, p 21-30. https://doi.org/10.1016/j.actamat.2017.10.035

17. S.A. Barannikova, A.M. Zharmukhambetova, A.Y. Nikonov, A.V. Dmitriev, A.V. Ponomareva, and I.A. Abrikosov, Influence of Stresses on Structure and Properties of Ti and Zr- Based Alloys from First-Principles Simulations, *IOP Conf. Ser. Mater. Sci.*

18. D.E. Smirnova, and S.V. Starikov, An Interatomic Potential for Simulation of Zr-Nb System, *Comput. Mater. Sci.*, 2017, **129**, p 259-272. https://doi.org/10.1016/j.commatsci.2016.12.016

19. Y. Zhao, H. Li, and Y. Huang, The Structure, Mechanical, Electronic and Thermodynamic Properties of Bcc Zr-Nb Alloy: A First Principles Study, *J. Alloys Compd.*, 2021, **862**, 158029. https://doi.org/10.1016/j.jallcom.2020.158029

20. A.R. Natarajan, P. Dolin, and A. Van Der Ven, Acta Materialia Crystallography, Thermodynamics and Phase Transitions in Refractory Binary Alloys, Elsevier Ltd, 2020, **200**, p 171-186.

21. W. Pfeiler, Investigation of Short-Range Order by Electrical Resistivity Measurement, *Acta Metall.*, 1988, **36**(9), p 2417-2434. https://doi.org/10.1016/0001-6160(88)90192-7

22. G. Kresse, and J. Furthmüller, Efficiency of Ab-Initio Total Energy Calculations for Metals and Semiconductors Using a Plane-Wave Basis Set, *Comput. Mater. Sci.*, 1996, **6**(1), p 15-50. https://doi.org/10.1016/0927-0256(96)00008-0

23. P. Giannozzi, S. Baroni, N. Bonini, M. Calandra, R. Car, C. Cavazzoni, D. Ceresoli, G.L. Chiarotti, M. Cococcioni, I. Dabo, A. Dal Corso, S. de Gironcoli, S. Fabris, G. Fratesi, R. Gebauer, U. Gerstmann, C. Gougoussis, A. Kokalj, M. Lazzeri, L. Martin-Samos, N. Marzari, F. Mauri, R. Mazzarello, S. Paolini, A. Pasquarello, L. Paulatto, C. Sbraccia, S. Scandolo, G. Sclauzero, A.P. Seitsonen et al., QUANTUM ESPRESSO: A Modular and Open-Source Software Project for Quantum Simulations of Materials, *J. Phys. Condens. Matter*, 2009, **21**(39), p 395502.

24. P. Giannozzi, O. Baseggio, P. Bonfà, D. Brunato, R. Car, I. Carnimeo, C. Cavazzoni, S. De Gironcoli, P. Delugas, F. Ferrari Ruffino, A. Ferretti, N. Marzari, I. Timrov, A. Urru, and S. Baroni, Quantum ESPRESSO toward the Exascale, *J. Chem. Phys.*, AIP Publishing, LLC, 2020, **152**(15), p 154105. https://doi.org/10.1063/5.0005082.

25. P. Giannozzi, O. Andreussi, T. Brumme, O. Bunau, M. Buongiorno Nardelli, M. Calandra, R. Car, C. Cavazzoni, D. Ceresoli, M. Cococcioni, N. Colonna, I. Carnimeo, A. Dal Corso, S. de Gironcoli, P. Delugas, R.A. DiStasio, A. Ferretti, A. Floris, G. Fratesi, G. Fugallo, R. Gebauer, U. Gerstmann, F. Giustino, T. Gorni, J. Jia, M. Kawamura, H.-Y. Ko, A. Kokalj, E. Küçükbenli, M. Lazzeri et al., Advanced Capabilities for Materials Modelling with Quantum ESPRESSO, *J. Phys. Condens. Matter*, 2017, **29**(46), p 465901. https://doi.org/10.1088/1361-648X/aa8f79

26. P.W. Tasker, The Stability of Ionic Crystal Surfaces, *J. Phys. C Solid State Phys.*, 1979, **12**(22), 4977, (3), p 3865-3868.

27. J.P. Perdew, K. Burke, and M. Ernzerhof, Generalized Gradient Approximation Made Simple, *Phys. Rev. Lett.*, 1996, p 3865-3868, https://doi.org/10.1103/PhysRevLett.77.3865.

28. B. Walker, and R. Gebauer, Ultrasoft Pseudopotentials in Time-Dependent Density-Functional Theory, *J. Chem. Phys.*, 2007, **127**(16), p 164106. https://doi.org/10.1063/1.2786999

29. A.P. Bartók, and J.R. Yates, Ultrasoft Pseudopotentials with Kinetic Energy Density Support: Implementing the Tran-Blaha Potential, *Phys. Rev. B*, 2019, **99**(23), p 235103. https://doi.org/10.1103/PhysRevB.99.235103

30. M. Methfessel, and A.T. Paxton, High-Precision Sampling for Brillouin-Zone Integration in Metals, *Phys. Rev. B*, 1989, **40**(6), p 3616-3621. https://doi.org/10.1103/PhysRevB.40.3616

31. J.M. Sanchez, Cluster Expansion and the Configurational Theory of Alloys, *Phys. Rev. B*, American Physical Society, 2010, **81**(22), p 224202, https://doi.org/10.1103/PhysRevB.81.224202.

32. A.T. Dinsdale, SGTE Data for Pure Elements, *Calphad*, 1991, **15**(4), p 317-425. https://doi.org/10.1016/0364-5916(91)90030-N

33. O. Redlich and A.T. Kister, Algebraic Representation of Thermodynamic Properties and the Classification of Solutions, *Ind.*

286

J. Phase Equilib. Diffus. (2022) 43:277–286

Eng. Chem., American Chemical Society, 1948, **40**(2), p 345-348, https://doi.org/10.1021/ie50458a036.

34. G. Inden, Atomic Ordering, in *Phase Transformations in Materials*, G. Kostorz, Ed., (WILEY-VCH, Weinheim, 2001), https://doi.org/10.1002/9783527603978.mst0391.

35. S. Lele, and B.N. Sarma, Computational Thermodynamics of Sc-Zr and Sc-Ti Alloys Using Cluster Variation Method, *J. Mater. Sci.*, 2009, **44**(9), p 2334-2342. https://doi.org/10.1007/s10853-008-3197-6

36. W.H. Press, S.A. Teukolsky, W.T. Vetterling, and B.P. Flannery, *Numerical Recipes in C: The Art of Scientific Computing*, (Cambridge University Press, Cambridge, 1993).

37. V. Jindal, B.N. Sarma, and S. Lele, A Thermodynamic Assessment of the Cr-Mo System Using CE-CVM, *Calphad*, 2013, **43**, p 80-85. https://doi.org/10.1016/j.calphad.2013.10.003

38. K. Lejaeghere, G. Bihlmayer, T. Bjorkman, P. Blaha, S. Blugel, V. Blum, D. Caliste, I.E. Castelli, S.J. Clark, A. Dal Corso, S. de Gironcoli, T. Deutsch, J.K. Dewhurst, I. Di Marco, C. Draxl, M. Du ak, O. Eriksson, J.A. Flores-Livas, K.F. Garrity, L. Genovese, P. Giannozzi, M. Giantomassi, S. Goedecker, X. Gonze, O. Granas, E.K.U. Gross, A. Gulans, F. Gygi, D.R. Hamann, P.J. Hasnip, et al., Reproducibility in Density Functional Theory Calculations of Solids. *Science (80-.).*, 2016, **351**(6280), p aad3000-aad3000, https://doi.org/10.1126/science.aad3000.

39. C. Kittel, *Introduction to Solid State Physics*, 8th edn. (Wiley, New York, 2004).

40. Y. Zhao, J. Zhang, C. Pantea, J. Qian, L.L. Daemen, P.A. Rigg, R.S. Hixson, G.T. Gray, Y. Yang, L. Wang, Y. Wang, and T. Uchida, Thermal Equations of State of the α, β, and ω Phases of Zirconium, *Phys. Rev. B*, 2008, **71**(18), p 184119. https://doi.org/10.1103/PhysRevB.71.184119

41. B.-T. Wang, P. Zhang, H.-Y. Liu, W.-D. Li, and P. Zhang, First-Principles Calculations of Phase Transition, Elastic Modulus, and Superconductivity under Pressure for Zirconium, *J. Appl. Phys.*, 2011, **109**(6), p 063514. https://doi.org/10.1063/1.3556753

42. C. Colinet, A. Pasturel, and P. Hicter, Trends in Cohesive Energy of Transition Metal Alloys, *Calphad*, 1985, **9**(1), p 71-99. https://doi.org/10.1016/0364-5916(85)90032-X

43. A. van de Walle, and G. Ceder, Automating First-Principles Phase Diagram Calculations, *J. Phase Equilibria*, 2002, **23**(4), p 348-359. https://doi.org/10.1361/105497102770331596

44. J. Gao, C. Li, J. Dang, C. Guo, and Z. Du, Experimental Determination and Thermodynamic Description of the Nb-V Binary System, *J. Alloys Compd.*, 2018, **768**, p 316-322. https://doi.org/10.1016/j.jallcom.2018.07.254

45. B.E. Warren, *X-Ray Diffraction* (Addison-Wesley, Reading, 1969).